Progress In Electromagnetics Research M, Vol. 32, 115–127, 2013

QUASI-OPTICAL FREQUENCY SELECTIVE SURFACE FOR ATMOSPHERIC REMOTE SENSING APPLICATION

Bu Gang Xia[1, 2, *], De Hai Zhang[1], Jian Huang[1, 2], and Jin Meng[1, 2]

[1]Key Lab of Microwave Remote Sensing, Centre for Space Science and Applied Research, Chinese Academy of Sciences, Beijing 100190, China

[2]University of Chinese Academy of Sciences, Beijing 100049, China

Abstract—The design of an efficient quasi-optics Frequency Selective Surface (FSS) filter which is required to provide a −3 dB pass band from 405 GHz to 441 GHz is presented. For atmospheric remote sensing application, this space-borne spatial device consists of a silicon layer and a thin copper layer which is perforated with periodic arrays of resonant dipole slots and circular apertures. FSS unit cell has a dimension much smaller than its operating wavelength. Unique features of this complex dense FSS structure include wide pass band properties with superb performance of frequency response and incident angles independence for TE polarization. Floquet mode analysis and finite element method (FEM) models are used to establish the geometry of the periodic structure and predict its spectral response.

1. INTRODUCTION

Intensive studies of Frequency Selective Surfaces (FSSs) [1, 2] start from the 1960's [3] because of the great potential for military applications in forming radome. In the past twenty years, passive remote sensing instrument technology has greatly been driven by the need to acquire spectroscopic characteristics of the Earth's atmosphere for studies including atmospheric composition, marine environmental monitoring and climatic oscillation.

Achieving high receiver sensitivity is required to detect weak molecular radiations at millimeter and sub-millimeter wavelengths. For

Received 23 June 2013, Accepted 30 July 2013, Scheduled 31 July 2013

* Corresponding author: Bu Gang Xia (xiabugang09@mails.ucas.ac.cn).

space science missions, full power radiometers are working over a wide frequency range. The signals are separated within the radiometers by quasi-optics [4] FSSs, which face severe challenges to provide low signal insertion loss and meet the conflictive requirement for high isolation between adjacent frequency channels.

Many successful precedents of FSSs employed by space-borne or air-borne radiometers can be listed, such as AMSU-B [5] launched by NOAA (National Oceanic and Atmospheric Administration) in 1996, which operates in three Gaussian Beam channels respectively centered at 89 GHz, 150 GHz and 183 GHz. MARSCHALS, the multichannel atmospheric limb sounding instrument of ESA (European Space Agency) in the range of 294–380 GHz, make use of quasi-optics FSSs, which consist of printed metallic arrays on fused silica substrates [6]. The freestanding dipole FSS centered at 448 GHz has recently been developed to satisfy the needs of the Microwave Imager Instrument (MWI). This passive radiometer mainly concentrates on atmospheric applications is a part of the Post EPS mission [7] in the 2018.

In this paper, a novel FSS — a conflicting design with constraints of very low insertion loss (< 0.3 dB) and high isolation (> 20 dB) between closely spaced frequency channels for TE polarized wave at either normal or oblique incidence is exploited to create. As a representative frequency point on O_2 absorption lines [8], 424 GHz is the center frequency of this proposed quasi-optics FSS filter which is an indispensable component for passive microwave remote sensing instruments such as sub-millimeter radiometer.

2. THEORETICAL ANALYSIS

Gaussian Beam Propagation (GBP) [9] is the fundamental theory of quasi-optics technology. In quasi-optical multiple-channel networks, the resonant mode of FSS can be described particularly by GBP transmission properties of EM wave in sub-millimeter range. Generally, changes are complicated in amplitude of EM wave (with the exception of plane wave in the ideal case). Only by solving the Maxwell's Equations according to relevant boundary conditions, the changes of amplitude can be calculated. However, the problem can be simplified by using the Paraxial Wave Equation (PWE) [10]. Under the circumstance that most of the energy is concentrated around the transfer axis when the EM wave is in the process of transmission, and in rectangular coordinates, the PWE for component of E-field is:

$$\frac{\partial^2 \zeta}{\partial x^2} + \frac{\partial^2 \zeta}{\partial y^2} - 2jk\frac{\partial \zeta}{\partial z} = 0 \tag{1}$$

where ζ is the complex scalar function that defines the non-plane part of the Gaussian Beam. Supposing the direction of propagation be in the positive Z orientation (shown in Figure 1), the fundamental Gaussian Beam mode of E-field distribution with the paraxial approximation in rectangular coordinates (two dimension) is shown in Equation (2):

$$E(x,y,z) = \sqrt{\frac{2}{\pi\omega_x\omega_y}} \cdot \exp\left(-\frac{x^2}{\omega_x^2} - \frac{y^2}{\omega_y^2}\right) \cdot \exp\left(-j\frac{\pi x^2}{\lambda R_x} - j\frac{\pi y^2}{\lambda R_y}\right) \cdot \exp\left(+j\frac{\sigma_{0x}}{2} + j\frac{\sigma_{0y}}{2} - jkz\right) \quad (2)$$

where

$$\omega_i = \omega_{0i}\left[1 + \left(\frac{\lambda z}{\pi\omega_{0i}^2}\right)^2\right]^{0.5} \quad (3)$$

$$R_i = z + \frac{1}{z}\left(\frac{\pi\omega_{0i}^2}{\lambda}\right) \quad (4)$$

$$\tan\sigma_{0i} = \frac{\lambda z}{\pi\omega_{0i}^2} \quad (5)$$

It can be seen from Equation (3) that ω_i ($i = x, y$) is defined as beam radius, the value of the radius at which the field falls to $1/e$ relative to its on-axis value. In particular, ω_{oi} is the minimum value of the beam radius, and it denotes the beam waist radius at where Z=0. Equations (4) and (5) demonstrate R_i (i.e., the curvature radius) and the Gaussian beam phase shift σ_{oi}, respectively. Solutions to the PWE are the Gaussian beam modes, which form the basis of quasi-optical system design.

To predict the interlayer transfer characteristics of quasi-optical FSS with arbitrarily shaped aperture arrays, the Floquet modes are analyzed. Fundamentally, Floquet modes are groups of plane waves with propagation direction set by the topology and frequency of the periodical arrays, and used to represent the fields on the port boundary. The Floquet modes are used solely with planar periodic arrays such as FSS and planar phased arrays which are idealized to infinitely large. The transmission characteristics of the infinite structures are then achieved by analyzing a FSS unit cell. Connected boundaries generally compose the side walls of a unit cell; however, to describe the boundary to infinite space, at least one "open" boundary condition is necessary. Just as Wave modes, Floquet modes have propagation constants and go through cut-off at an adequately low frequency. When a Floquet mode is present, it performs a modal decomposition

which gives additional information on the frequency performance of the radiated structure. This information is computed in the form of an S-matrix inter-relating the Floquet modes, as in the case of a Wave mode. As a matter of fact, if Floquet modes and Wave modes are concurrently present, the S-matrix will inter-relate all Wave modes and Floquet modes in the model of FSS unit cell. Floquet modes analysis, the eigenmodes of the periodic FSS structure, is indispensable to decompose the fields of input and output arrays into the forward and the backward propagating filed components. Moreover, transmission modes and evanescent modes are discussed in detail as well. Given the propagation constant k_o, and as shown in Figure 1, angle of incidence and polarizing angle are θ and φ, respectively. W and V are two directions of arrays, and α is the arrangement angle of W and V. Simultaneity, D_w and D_v represent the unit cell period of each direction. Then, we can write the wave vector:

$$\psi = k_o \sin\theta\cos\varphi\hat{x} + k_o \sin\theta\sin\varphi\hat{y} + k_o\cos\theta\hat{z} \tag{6}$$

When arrangement angle $\alpha = 60°$, Floquet modes maintain that the operated region for calculating the wave propagation features can be reduced to analysis a periodical FSS unit cell. On the basis of Floquet theorem [11, 12], the formulation of scalar Floquet modes [13]

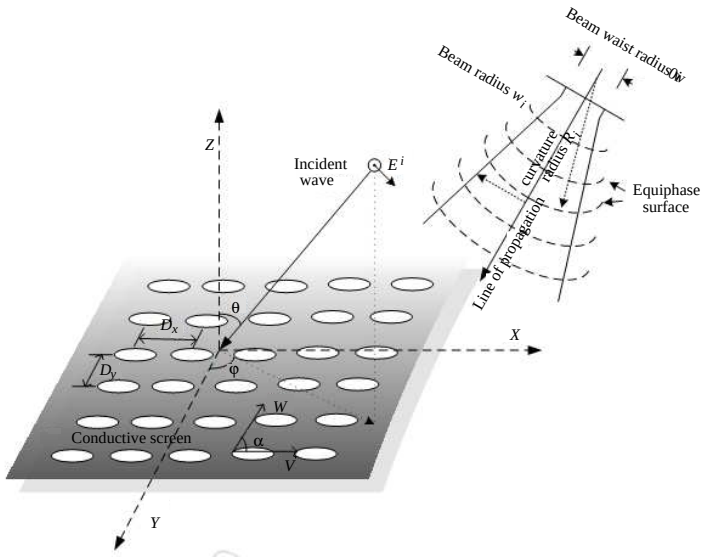

Figure 1. Quasi-optical FSS with arbitrarily shaped apertures excited by an oblique Gaussian Beam.

is given by:

$$\Theta_{mn} = \exp\left[-j\left(k_o \sin\theta\cos\varphi + \frac{2\pi m}{D_w}\right)x\right] \cdot \exp\left(-jk_o \sin\theta \sin\varphi\right) y \cdot \exp\left(-j\frac{2\pi n}{D_v \sin\alpha} - \frac{2\pi m}{D_w \tan\alpha}\right) y \cdot \exp\left(-j\Gamma_{mn} z\right) \quad (7)$$

where

$$\Gamma_{mn} = \begin{cases} \sqrt{k^2 - \rho_{mn}^2} & \left\langle k^2 > \rho_{mn}^2 \right\rangle \\ -j\sqrt{\rho_{mn}^2 - k^2} & \left\langle \rho_{mn}^2 > k^2 \right\rangle \end{cases} \quad (8)$$

And

$$\rho_{mn}^2 = \left(k_o \sin\theta \sin\varphi + \frac{2\pi n}{D_v \sin\alpha} - \frac{2\pi m}{D_w \tan\alpha}\right)^2 + \left(k_o \sin\theta\cos\varphi + \frac{2\pi m}{D_w}\right)^2 \quad (m, n = 0, \pm 1, \pm 2 \ldots, +\infty). \quad (9)$$

When Γ_{mn} is a real positive number, Floquet modes have phase changes along the direction of propagation. Corresponding to a plane wave radiation, it is known as transmission mode. Nevertheless, the shift of phase will be only perpendicular to the direction of propagation if Γ_{mn} is a pure imaginary number when the amplitude is in reduction, and it is called attenuation mode. Dominant mode of Floquet mode can be defined in condition of $m = n = 0$; otherwise (e.g., $m \neq 0$ or $n \neq 0$), the radiation beam can be expressed as grating lobe [14]. Counted by mathematical method of separation of variables, Floquet mode are, essentially, solutions of electromagnetic field equation with periodic boundary conditions. FSS consists of periodic electromagnetic resonance arrays, and its radiation field can be elaborated by utilizing a set of Floquet modes.

3. DESIGN TECHNIQUE

Unlike FSS arrays which simply consist of freestanding metal apertures or strips, this quasi-optical spatial filter is a substrate-based FSS [15, 16] with periodic unit cells. This type of FSS can easily be designed to operate at oblique incident angles and band pass modes. Meanwhile, according to the performance requirements of design indicators, this FSS should exhibit minimum insertion loss at $f_p = 424{\sim}426\,\text{GHz}$, and regulate a stop-band attenuation larger than 20 dB at $f_s = 480{\sim}500\,\text{GHz}$. The design approach to achieve this satellite-borne device is demonstrated in this section.

As shown in Figure 2, an individual unit cell of quasi-optics FSS contains two joint layers: a 4 μm copper layer, perforated periodically

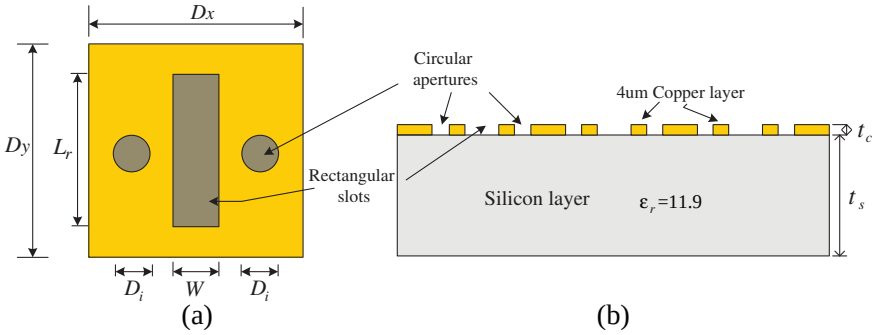

Figure 2. Geometry and dimensions of FSS. (a) Plan view of unit cell. (b) Side view of the filter's structure.

with rectangular dipole slots coupled with circular aperture elements on each side. The copper layer is structured on an electrically thick silicon wafer layer (relative dielectric permittivity $\varepsilon_r = 11.9$). Silicon is a suitable choice as backing material for space science applications since it is rigid, extremely low dielectric loss [7, 17] (Loss tangent $\tan\delta = 0.00001 \sim 0.0001$) and high resistivity even at terahertz wave range. Furthermore, it also can be burnished to provide an optically smooth surface. The structural geometry and dimensions of unit cell must be numerically calculated. The equation, which thickness of silicon wafer [18, 19] has to fit is proposed as follow:

$$t_s = \tau \cdot \frac{D_x^2}{D_y L_\gamma} \cdot \cos\left[\arcsin\left(\frac{\sin\theta}{\sqrt{\varepsilon_r}}\right)\right] \cdot \frac{c}{2f_{pass}\sqrt{\varepsilon_r}} \quad \langle \tau = 1, 2, 3 \ldots \rangle \quad (10)$$

where

$$L_\gamma = \frac{c}{2f_{pass}\sqrt{\varepsilon_e}} = \frac{c}{2f_{pass}\sqrt{\frac{1+\varepsilon_r}{2}}} \quad (11)$$

where c is the speed of the light in vacuum and ε_e the effective dielectric permittivity, approximately given by $\varepsilon_e = (1+\varepsilon_r)/2$. In addition, ratio is chosen at $\tau = 2$. And L_γ is the length of rectangular dipole slot. Also, by Equation (11), $L_\gamma = 139\,\mu\text{m}$ can be figured out. According to [20], the required size of unit cell results in $D_x = D_y = 166\,\mu\text{m}$, where $D_x = D_y$ is the periodicity of the unit cell shown in Figure 2(a). On the basis of calculations above, the thickness of silicon wafer is available by consulting to Equation (10), $t_s = 250\,\mu\text{m}$, under specified condition that $f_p = 424\,\text{GHz}$. Moreover, the value of slot width is set to $W = 32\,\mu\text{m}$. For manufacturing repeatability $\pm 1.4\,\mu\text{m}$ ($< 0.002\lambda_o$) is an acceptable tolerance on the slot length L_γ, and for the width

W, periodicity $D_x = D_y$ with an uncertainty of $\pm 3.5\,\mu\text{m}$ ($< 0.005\lambda_o$) is acceptable. Because of the large relative dielectric permittivity (i.e., $\varepsilon_r = 11.9$), the influences due to fabrication tolerance and the variation of incident angle will be decreased. Furthermore, the new design of FSS generates a broader pass band, a reduced insertion loss in the transmission band and a great symmetry property because of the increase in duty ratio which is obtained by these two circular apertures on both sides of the dipole slot. This will be particularly analyzed in the next section.

4. RESULTS AND OPTIMIZATION

To study the transmission characteristics of this newly designed FSS and obtain the optimal dimensions and parameters of the structure, numerical simulations are performed to verify the design methods elaborated above. The result shows that this FSS design has an excellent performance in the whole frequency band. Additionally, the frequency domain Finite Element Method (FEM) solver [21] is used because the FSS is designed to operate at oblique incidence wave. The FSS array is modeled with Floquet ports and periodic boundary conditions to provide Gaussian Beam at normal incidence and 45° incidence for TE polarization, respectively.

The spectral response of the quasi-optics FSS is clearly explained in Figure 3. From the transmission curve, it can be seen that the resonance occurs at 425.2 GHz for TE excitation (when $\theta = 0°$, $\alpha = 90°$, $\varphi = 0°$), and the power conversion efficiency $P_t = 0.9419$ with an insertion loss $\Delta P = -0.26\,\text{dB}$. The inner figure at upper-left corner shows the $-3\,\text{dB}$ pass band of $BW_{-3\,\text{dB}} = 36\,\text{GHz}$ (approx. from 405 GHz to 441 GHz).

There will be a slight alteration towards the resonant frequency compared with the theoretical result. This alteration arises from surface roughness inside the apertures and slots, which is also the reason for the reduced maximum power conversion efficiency $P_t = 0.9419$. An additional cause for the reduced transmittance is ohmic loss, especially over the sub-millimeter range.

In Figure 4, the phase shift characteristic which corresponds with the transmission response shown in Figure 3 is plotted. In the frequency range of 0∼500 GHz, the phase shifts periodically from 180° to −180°. Simultaneously, as observed from this figure, the phase decreases within the 3 dB bandwidth: at 405 GHz, the phase is less than −90°, and at 441 GHz, the value is −180°.

Resonant frequency (i.e., 425.2 GHz) is also the midpoint of phase shift, at about 136.1°. Theoretically [22], the phase of may be stabilized

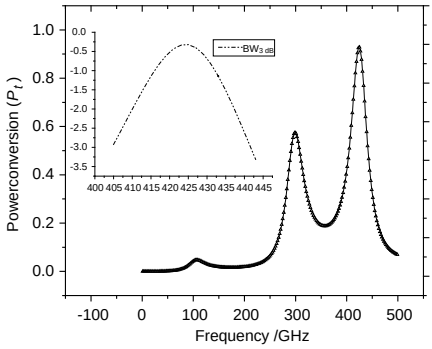

Figure 3. Transmission factor of FSS screen excited by normal incident wave for TE polarization.

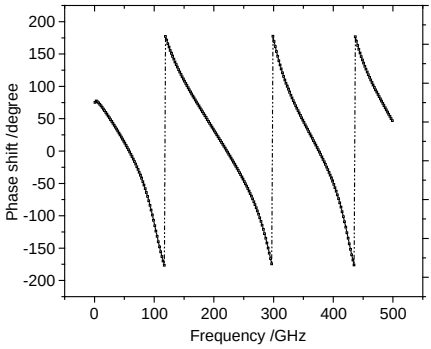

Figure 4. Phase shift characteristic.

at around $-180°$ in higher frequency (> 441 GHz). But according to Figure 4, the phase varies irregularly, mainly due to the existence of the grating lobe, and the method of eliminating grating lobe is explicitly stated in the following part.

The evolutionary FSS exhibits much better performance than the FSS that merely contains rectangular slots. Structurally, the 4 μm thin circular apertures arrays play an important role for this performance. Due to the existence of two circular apertures which distribute perpendicular to the dipole slot in each unit cell, excellent FSS transmission character is achieved. For application to submillimeter receiver systems, this quasi-optical FSS operates centered at about 425 GHz, so corresponding dimension of FSS unit cell is subwavelength (i.e., less than 1 μm), and its fabrication usually requires specialized and sophisticated technologies, resulting in time-consuming and expensively machining technology. Thus, to achieve the required FSS filtering response and reduce fabrication tolerance using a simplest structure with rotationally symmetrical geometries, the circle elements which can offer good angle incident stability are considered. As shown in Table 1, the main parameters of the transmission characteristics change continually with the increase of D_i (i.e., diameter of circular aperture).

The FSS is provided with 3 dB bandwidth of 28 GHz, an insertion loss of -1.46 dB, and operating frequency of 422.7 GHz, which does not comply with required design objectives. Fortunately, the transmission characteristic is getting better since the diameter of circular apertures getting larger and larger. However, it is not the bigger the better. For instance, when D_i increased from 30 μm to 36 μm, the power

Table 1. Variation tendency of FSS transmittance properties (when the diameter D_i changed from 0 μm to 42 μm).

f_p/GHz	$BW_{-3\,\mathrm{dB}}$ /GHz	ΔP/dB	P_t	α/°	θ/°	D_i/μm
422.7	28	−1.46	0.7142	90	0	0
423.1	31	−0.65	0.8615			12
423.5	33	−0.55	0.8802			18
424.9	34	−0.42	0.9071			24
425.2	36	−0.26	0.9419			30
423.9	32	−0.40	0.9113			36
423.6	31	−0.55	0.8807			42

conversion efficiency P_t reduced from 0.9419 to 0.9113, not as expected. Simulation result shows that the optimal value is $D_i = 30$ μm, as shown in Table 1.

The E field distributions of resonant frequency are reported in Figure 5, as well as the H field distributions. According to Figure 5(a), it is noted that the feature of the electric field distribution while FSS filter is at the peak of resonance ($f_p = 425.2$ GHz). Electric field mainly concentrates on the central region, and it gradually decreases from inside to outside of the screen. On the contrary, from Figure 5(b), it can be found that the magnetic field mostly gathers at the two terminals of dipole slot.

Performance of polarization and incident angles independence is

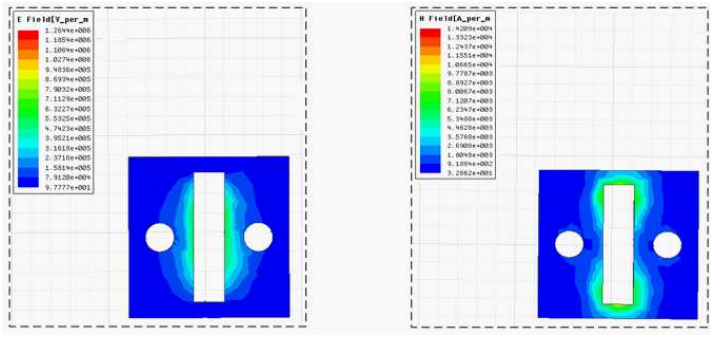

Figure 5. Field distributions. (a) E field distribution. (b) H field distribution.

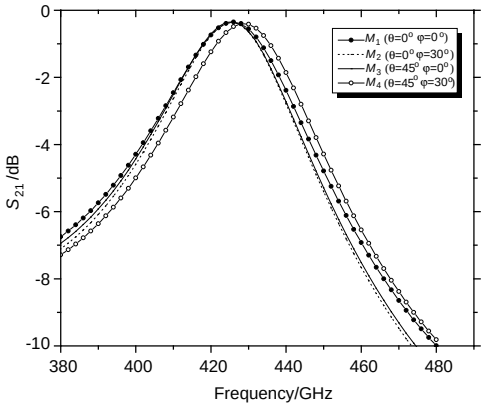

Figure 6. Change trend analysis of transmission coefficient for FSS in FEM model at TE polarization.

described in Figure 6. In order to facilitate analysis, a set of points (M_1, M_2, M_3, M_4) are divided into four groups, i.e., (M_1, M_2), (M_3, M_4), (M_1, M_3) and (M_2, M_4). Then an common phenomenon in (M_1, M_2), (M_3, M_4) is discovered: on the condition that incident angle θ remains unchanged, if φ increases, the resonant frequencies will increase as well; meanwhile, the loss will decrease, and pass-band will remain unchanged. For example, if φ changes from 0° to 30° (when $\theta = 45°$), f_p increases by 1.5 GHz, ΔP dwindles by 0.14 dB. On the other hand, considering (M_1, M_3) and (M_2, M_4), we notice that with larger incident angle (φ is invariant), the resonant frequency becomes higher, and the loss increases instead. By analyzing the (M_2, M_4) in Figure 6, it can be found that the resonant frequency f_p shifts from 426.1 GHz to 428.3 GHz and that ΔP rises from −0.36 dB to −0.41 dB.

Figure 7(a) shows the S_{21} curve of FSS when the arrangement angle $\alpha = 90°$, on this particular occasion, $f_p = 425.2$ GHz, $\Delta P = -0.26$ dB, grating lobe appears at around 558 GHz. But if the arrangement angle [23] changes to $\alpha = 60°$, the resonance point will be cut by 0.6 GHz (much closer to the required value 424 GHz), and the insertion loss will reduce from −0.26 dB to −0.19 dB, which means a better energy transmission capability. And the 3 dB pass band is also widen when comparing the two inner figures of Figures 7(a) and (b). At the same time, the appearance of grating lobe is delayed to more than 600 GHz. On the basis of analysis above, it can be seen that the important effect of arrangement cannot be neglected. Careful design of the structure can gain desired characteristics. In this case, 60° is a better choice than 90°.

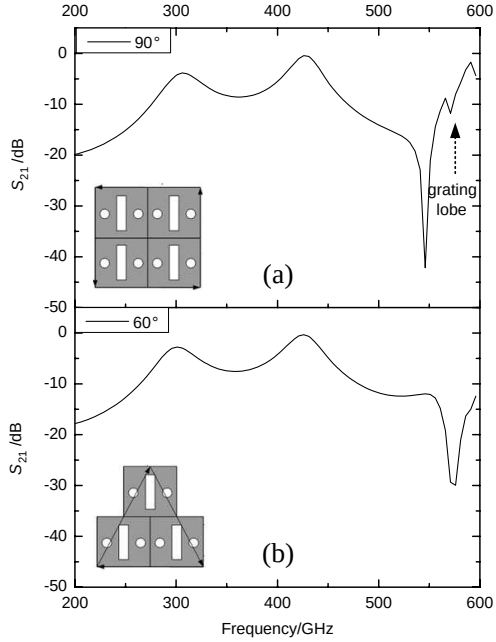

Figure 7. Effect of arrangement to the transmission characteristic of FSS. (a) Unit cell with square lattice. (b) Unit cell with equilateral triangular lattice.

5. CONCLUSION

The design of a substrate based quasi-optics FSS is described in this paper, where a high transmissivity is achieved without incurring larger insertion loss which limits the performance of existing spatial filter architectures. The behavior of the FSS filter is investigated by using GBP theory and FEM computer model, and the importance of including the effects of circular apertures and unit arrangement is demonstrated in detail. This type of low loss quasi-optical FSS can do some contribution in the next generation of space borne radiometers to enhance to their performance in space science missions.

REFERENCES

1. Munk, B. A., *Frequency Selective Surfaces: Theory and Design*, Wiley, New York, 2000.
2. Martinez-Lopez, R., J. Rodriguez-Cuevas, A. E. Martynyuk, and

J. I. Martinez-Lopez, "An active ring slot with RF MEMS switchable radial stubs for reconfigurable frequency selective surface applications," *Progress In Electromagnetics Research*, Vol. 128, 419–440, 2012.

3. Chen, C. C., "Transmission through a conducting screen perforated periodically with apertures," *IEEE Transactions on Microwave Theory and Techniques*, Vol. 18, 627–632, 1970.
4. Dragoman, D. and M. Dragoman, "Terahertz fields and applications," *Progress in Quantum Electronics*, Vol. 28, 1–66, 2004.
5. Dickie, R., R. Cahill, H. S. Gamble, V. F. Fusco, A. G. Schuchinsky, and N. Grant, "Spatial demultiplexing in the submillimeter wave band using multilayer free-standing frequency selective surfaces," *IEEE Transactions on Antennas and Propagation*, Vol. 53, 1904–1911, 2005.
6. Oldfield, M., B. Moyna, E. Allouis, R. Brunt, U. Cortesi, B. Ellison, J. Ellison, J. Eskell, T. Forward, T. Jones, D. Lamarre, J. Langen, P. de Maagt, D. Matheson, I. Morgan, J. Reburn, and R. Siddan, "MARSCHALS: Development of an airborne millimeter-wave limb sounder," *International Symposium on Remote Sensing, International Society for Optics and Photonics*, 221–228, 2001.
7. Peubey, C., W. Bell, P. Bauer, and S. D. Michele, *A Study on the Spectral and Radiometric Specifications of a Post-eps Microwave Imaging Mission,* European Centre for Medium-Range Weather Forecasts, 2011.
8. Xia, B. G., J. Meng, D. H. Zhang, and J. S. Zhang, "PMM-GA method to synthesize quasi-optical frequency selective surface on SiO_2 substrate," *Progress In Electromagnetics Research*, Vol. 139, 599–610, 2013.
9. Goldsmith, P. F., *Quasi-optical Systems: Gaussian Beam Quasi-optical Propagation and Applications*, IEEE Press, Piscataway, 1998.
10. Rebecca, H. J. and D. G. Hall, "Free-space azimuthal paraxial wave equation: The azimuthal Bessel-Gauss beam solution," *Optics Letters*, Vol. 19, 427–429, 1994.
11. Kuchment, P. A., "Floquet theory for partial differential equations," *Russian Mathematical Surveys*, Vol. 37, 1–60, 1982.
12. Sorokin, S. V. and O. A. Ershova, "Analysis of the energy transmission in compound cylindrical shells with and without internal heavy fluid loading by boundary integral equations and by Floquet theory," *Journal of Sound and Vibration*, Vol. 291,

81–99, 2006.

13. Watanabe, K. and K. Yasumoto, "Accuracy improvement of the Fourier series expansion method for Floquet-mode analysis of photonic crystal waveguides," *Progress In Electromagnetics Research*, Vol. 92, 209–222, 2009.
14. Lu, B., S. X. Gong, S. Zhang, Y. Guan, and J. Ling, "Optimum spatial arrangement of array elements for suppression of grating-lobes of radar cross section," *IEEE Antennas and Wireless Propagation Letters*, Vol. 9, 114–117, 2010.
15. Costa, F., A. Monorchio, and G. Manara, "Analysis and design of ultra thin electromagnetic absorbers comprising resistively loaded high impedance surfaces," *IEEE Transactions on Antennas and Propagation*, Vol. 58, 1551–1558, 2010.
16. Zhang, J. C., Y. Z. Yin, and R. Yi, "Resonant characteristics of frequency selective surfaces on ferrite substrates," *Progress In Electromagnetics Research*, Vol. 95, 355–364, 2009.
17. Monacelli, B., J. B. Pryor, B. A. Munk, D. Kotter, and G. D. Boreman, "Infrared frequency selective surface based on circuit-analog square loop design," *IEEE Transactions on Antennas and Propagation*, Vol. 53, 745–752, 2005.
18. Lee, J. W., M. A. Seo, D. S. Kim, S. C. Jeong, C. Lienau, J. H. Kang, and Q. Park, "Fabry-Perot effects in THz time-domain spectroscopy of plasmonic band-gap structures," *Applied Physics Letters*, Vol. 88, 071114-1–071114-3, 2006.
19. Takakura, Y., "Optical resonance in a narrow slit in thick metallic screen," *Physical Review Letters*, Vol. 86, 5601–5603, 2001.
20. Reed, J. A. and D. M. Byrne, "Frequency-selective surfaces with multiple apertures within a periodic cell," *Journal of the Optical Society of America*, Vol. 15, 660–668, 1997.
21. Bardi, I., R. Remski, D. Perry, and Z. Cendes, "Plane wave scattering from frequency-selective surfaces by the finite-element method," *IEEE Transactions on Magnetics*, Vol. 38, 641–644, 2002.
22. Winnewisser, C., F. Lewen, J. Weinzierl, and H. Helm, "Transmission features of frequency-selective components in the far infrared determined by terahertz time-domain spectroscopy," *Applied Optics*, Vol. 38, 3961–3976, 1999.
23. Kiani, G. I., K. L. Ford, K. P. Esselle, A. R. Weily, and C. J. Panagamuwa, "Oblique incidence performance of a novel frequency selective surface absorber," *IEEE Transactions on Antennas and Propagation*, Vol. 55, 2931–2934, 2007.